2011

Vacuolization of mucolipidosis type II mouse exocrine gland cells represents accumulation of autolysosomes

Marielle Boonen
Washington University School of Medicine in St. Louis

Eline van Meel
University Medical Center Utrecht

Viola Oorschot
University Medical Center Utrecht

Judith Klumperman
University Medical Center Utrecht

Stuart Kornfeld
Washington University School of Medicine in St. Louis

Vacuolization of mucolipidosis type II mouse exocrine gland cells represents accumulation of autolysosomes

Marielle Boonen[a,*], Eline van Meel[b,*], Viola Oorschot[b], Judith Klumperman[b], and Stuart Kornfeld[a]
[a]Department of Internal Medicine, Washington University School of Medicine, St. Louis, MO 63110; [b]Department of Cell Biology, University Medical Center Utrecht, 3584 CX Utrecht, The Netherlands

ABSTRACT **We previously reported that mice deficient in UDP-GlcNAc:lysosomal enzyme GlcNAc-1-phosphotransferase (mucolipidosis type II or *Gnptab* −/− mice), the enzyme that initiates the addition of the mannose 6-phosphate lysosomal sorting signal on acid hydrolases, exhibited extensive vacuolization of their exocrine gland cells, while the liver, brain, and muscle appeared grossly unaffected. Similar pathological findings were observed in several exocrine glands of patients with mucolipidosis II. To understand the basis for this cell type–specific abnormality, we analyzed these tissues in *Gnptab* −/− mice using a combined immunoelectron microscopy and biochemical approach. We demonstrate that the vacuoles in the exocrine glands are enlarged autolysosomes containing undigested cytoplasmic material that accumulate secondary to deficient lysosomal function. Surprisingly, the acid hydrolase levels in these tissues ranged from normal to modestly decreased, in contrast to skin fibroblasts, which accumulate enlarged lysosomes and/or autolysosomes also but exhibit very low levels of acid hydrolases. We propose that the lysosomal defect in the exocrine cells is caused by the combination of increased secretion of the acid hydrolases via the constitutive pathway along with their entrapment in secretory granules. Taken together, our results provide new insights into the mechanisms of the tissue-specific abnormalities seen in mucolipidosis type II.**

Monitoring Editor
Robert G. Parton
University of Queensland, Australia

Received: Jul 12, 2010
Revised: Jan 10, 2011
Accepted: Feb 7, 2011

INTRODUCTION

Mucolipidosis type II (MLII, inclusion-cell disease or I-cell disease) is an autosomal recessive disorder due to deficiency of UDP-GlcNAc:lysosomal enzyme GlcNAc-1-phosphotransferase (GlcNAc-1-phosphotransferase), the first enzyme involved in the synthesis of the mannose 6-phosphate (Man-6-P) signal, which allows the specific targeting of lysosomal acid hydrolases from the *trans*-Golgi network (TGN) to lysosomes (Kornfeld and Sly, 2000; Pohl *et al.*, 2009; Cathey *et al.*, 2010; Kollmann *et al.*, 2010). The fibroblasts of MLII patients have been shown to hypersecrete most of their newly synthesized acid hydrolases via the constitutive secretory pathway, thereby accounting for the deficiency of acid hydrolases in these cells and, at least partially, for the high level of these same hydrolases in the extracellular fluids of the patients (Leroy and Demars, 1967; Lightbody *et al.*, 1971; Tondeur *et al.*, 1971; Wiesmann *et al.*, 1971a, 1971b; Hickman and Neufeld, 1972; Leroy *et al.*, 1972; Aula *et al.*, 1975; Martin *et al.*, 1975). At the morphological level, the most striking alterations have been found in these fibroblasts and other cell types of mesenchymal origin, which develop a lysosomal storage phenotype characterized by the accumulation of phase-dense inclusions that gave rise to the term "inclusion-cell disease" (Leroy and DeMars, 1967; Kenyon and Sensenbrenner, 1971; Aula *et al.*, 1975; Martin *et al.*, 1975; Nagashima *et al.*, 1977). By contrast, other cell types exhibit few, if any, morphological alterations, including most cells of the hepatic parenchyma, CNS, and muscle (Kenyon *et al.*, 1973; Martin *et al.*, 1975, 1984; Nagashima *et al.*, 1977). Interestingly, a more recent report described striking vacuolization at a

This article was published online ahead of print in MBoC in Press (http://www.molbiolcell.org/cgi/doi/10.1091/mbc.E10-07-0584) on February 16, 2011.

*These authors contributed equally to this work.

Address correspondence to: Stuart Kornfeld (skornfel@dom.wustl.edu).

Abbreviations used: CCV, clathrin-coated vesicle; EM, electron microscopy; FCS, fetal calf serum; GA, glutaraldehyde; GlcNAc-1-phosphotransferase, UDP-GlcNAc:lysosomal enzyme GlcNAc-1-phosphotransferase; *Gnptab*, gene encoding the alpha/beta subunits of GlcNAc-1-phosphotransferase; HRP, horseradish peroxidase; ISG, immature secretory granule; Man-6-P, mannose 6-phosphate; MLII, mucolipidosis type II; MPR, mannose 6-phosphate receptor; PB, phosphate buffer; PBS, phosphate-buffered saline; PFA, paraformaldehyde; PNS, postnuclear supernatant; RT, room temperature; TGN, *trans*-Golgi network.

novel site: the serous secretory cells of the pancreas and salivary glands of several infants with MLII (Elleder and Martin, 1998). In that study, the origin of the vacuoles was not explained and the acid hydrolase content of these tissues was not determined. During the course of studying mice mutant in the gene *Gnptab*, which encodes the α/β catalytic subunits of GlcNAc-1-phosphotransferase (MLII mouse model), we observed similar vacuolization in the exocrine secretory cell types (Gelfman *et al.*, 2007; Vogel *et al.*, 2009). This finding provided the opportunity to investigate the nature and cause of this pathological alteration.

In this article, we demonstrate that the vacuolization of the acinar cells of the pancreatic and salivary glands of *Gnptab* −/− mice (or MLII mice) seen by light microscopy represents the accumulation of numerous, large autolysosomes, involved in crino-, micro-, and macroautophagy. Interestingly, enzymatic assays revealed that these glands have only a modest decrease in acid hydrolase content, in contrast to the major deficiency exhibited by the skin fibroblasts derived from the mutant mice, in which we also detected an accumulation of enlarged lysosomes and/or autolysosomes by electron microscopy. On the basis of our findings and the current understanding of the special role of the Man-6-P recognition system in secretory cells, we propose that the lack of Man-6-P signals on the acid hydrolases results in their entrapment within exocrine gland secretory granules as well as increased secretion and, consequently, in lysosomal dysfunction. These results suggest that hypersecretion of acid hydrolases via the constitutive secretory pathway may not be the only cause for the development of lysosomal insufficiency in mucolipidosis II mice and patients.

RESULTS

Vacuolization of the acinar cells of the salivary glands and pancreas of *Gnptab* −/− mice represents accumulation of autolysosomes

The acini of the exocrine salivary glands, which consist of mucous- and serous-type secretory cells, exhibited extensive vacuolization in *Gnptab* −/− mice when examined by light microscopy (Gelfman *et al.*, 2007; Vogel *et al.*, 2009). To gain insight into the underlying pathology, we analyzed the submandibular salivary gland of these mice by electron microscopy (EM). Both mucous- and serous-type secretory cells were readily observed in the wild-type mice (Figure 1A). By contrast, the overall architecture of the submandibular salivary gland of the *Gnptab* −/− mice was so grossly disrupted that it greatly hampered the identification of the serous cells in the EM sections (Figure 1B). The mucous-type secretory cells, however, could be recognized by their characteristic electron lucent secretory granules (average diameter size ~800 nm). These cells were packed with large (up to ~4 μm in diameter) membrane-bound vacuoles that contained heterogeneous material (Figure 1B arrowheads, higher magnification in Figure 1C), which accounted for the extensive vacuolization observed by light microscopy. Detailed morphological analysis of these vacuoles in *Gnptab* −/− mucous cells showed that they often contained material reminiscent of undigested cytoplasmic organelles, particularly mitochondria (Figure 1D), suggesting a defect in the autophagic pathway.

Macroautophagy (hereafter referred to as autophagy), which is the most prevalent type of autophagy in most tissues, starts with the sequestration of cargo destined for degradation in a large double-membrane vesicle, the autophagosome. The fusion of the autophagosome with a lysosome gives rise to an autolysosome, where degradation of the cargo takes place (Cao and Klionsky, 2007). Recent studies of the lysosomal storage disorders "multiple sulfatase deficiency" and "mucopolysaccharidosis type IIIA" in mice reported the accumulation of autophagosomes in mouse embryonic fibroblasts and macrophages, resulting from defective autophagosome–lysosome fusion (Settembre *et al.*, 2008). We therefore asked whether a similar block in autophagy might be occurring in the *Gnptab* −/− submandibular gland. The large vacuoles filled with undegraded cytoplasmic material that accumulate in the *Gnptab* −/− mucous cells were surrounded by a single membrane (Figure 1, C and D) and, as shown in Figure 1D, LAMP-2 was readily detected by cryo-immunogold EM in their limiting membrane. These observations indicate that they represent autolysosomes formed by fusion of autophagic compartments with lysosomes. In this regard, these results differ from the accumulation of autophagosomes reported in the other lysosomal storage disorders.

Interestingly, we observed numerous fusion profiles of mucous granules with the autolysosomes, consistent with ongoing crinophagy, an autophagic process by which secretory granules directly fuse with lysosomes or autolysosomes (Figure 1, E and F, arrows) (Smith and Farquhar, 1966). We also found mucous secretory granules that were being engulfed by autolysosomes, a process described as microautophagy (Figure 1, E and G, arrowhead) (Cuervo, 2004).

In addition to the salivary gland, the exocrine pancreas of the *Gnptab* −/− mice also exhibited a clear vacuolization under the light microscope (Gelfman *et al.*, 2007; Vogel *et al.*, 2009). EM analysis revealed that the acinar cells of this organ, which are serous-type secretory cells, were similarly affected by the loss of the Man-6-P targeting pathway. In the wild-type pancreas, LAMP-2 localized to normal sized lysosomes with a diameter of ~300–600 nm (Figure 2A). By contrast, the *Gnptab* −/− serous cells exhibited an accumulation of large LAMP-2 positive compartments, which had an approximate diameter of 500 nm to 2 μm and were filled with undegraded cytoplasmic material (Figure 2, B-D). Mitochondrial remnants were regularly observed in the lumen of these compartments (Figure 2B) and undigested secretory granules were occasionally detected (Figure 2, C and D). Therefore, as in the salivary gland, these compartments could be identified as autolysosomes on the basis of their content and membrane protein composition. LAMP-2 negative autophagosomes were also occasionally observed (unpublished data). Consistent with the accumulation of LAMP-2 positive autolysosomes, the level of LAMP-2 as determined by Western blotting was markedly increased in the *Gnptab* −/− pancreas, as well as in the mutant parotid, sublingual, and submandibular salivary glands (Figure 3A). In contrast, the brain, liver, and muscle exhibited normal levels of LAMP-2 in the mutant mouse compared with wild-type (Figure 3A). Of note, the secretory granules in the *Gnptab* −/− pancreatic acinar cells appeared similar to those of the wild-type cells in shape and density (Figure 2, E and F) but were smaller in size (~27% smaller compared with wild type).

Gnptab −/− exocrine glands lack signs of a strong induction of macroautophagy

One mechanism that could lead to the accumulation of autolysosomes in the salivary and pancreatic glands of the *Gnptab* −/− mice would be an enhanced activation of the autophagy process that might overwhelm the lysosomal degradative capacity. To address this possibility, we determined the levels of Beclin-1 and the activity of the serine/threonine kinase mTOR (target of rapamycin) in the salivary glands and pancreas of the *Gnptab* −/− and wild-type mice. Beclin-1 and mTOR are key regulators in the process of macroautophagy (Pattingre *et al.*, 2008). Increased levels of Beclin-1, which is part of a PI(3)-kinase complex, activate and up-regulate the process of autophagy through its interaction with hVps34

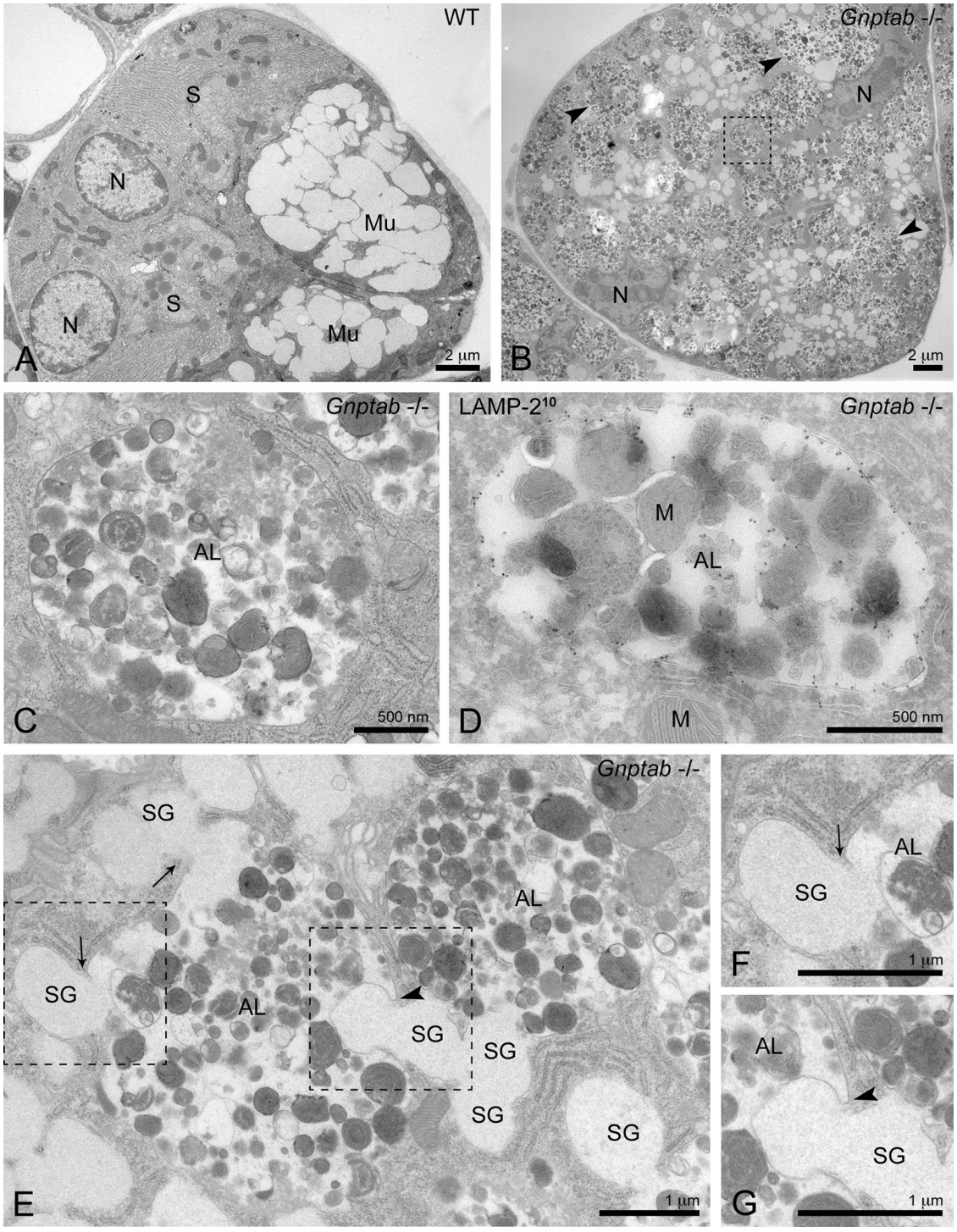

FIGURE 1: Autolysosomes accumulate in the submandibular salivary gland of *Gnptab* −/− mice. (A) Electron micrograph showing a low-magnification overview of a wild-type (WT) mouse submandibular salivary gland acinus, composed of mucous and serous cells. (B) Overview of a *Gnptab* −/− submandibular salivary gland acinus. The overall architecture is disrupted by the massive accumulation of large vacuoles with diameter sizes up to ~4 μm (arrowheads). Mucous-type secretory cells are recognized by the presence of the electron lucent secretory granules (average diameter size ~800 nm). (C) Higher magnification of a vacuole from (B), which is surrounded by a single membrane and contains undegraded material. Area of magnification is indicated by the box in (B). (D, E) Further characterization of the vacuoles that accumulate in the *Gnptab* −/− submandibular salivary gland shows the presence of the lysosomal membrane protein LAMP-2 in their limiting membrane by immunogold labeling (D, 10-nm gold particles), mitochondria inside their lumen (D), fusion with (E, arrows) and engulfment (E, arrowhead) of mucous secretory granules (crinophagy and microautophagy events, respectively). Taken together, these observations define these vacuoles as autolysosomes. Higher magnifications of the (F) crinophagy and (G) microautophagy events shown in (E). Areas of magnification are indicated by the boxes in (E). AL, autolysosome; M, mitochondrion; Mu, mucous cell; N, nucleus; S, serous cell; SG, secretory granule.

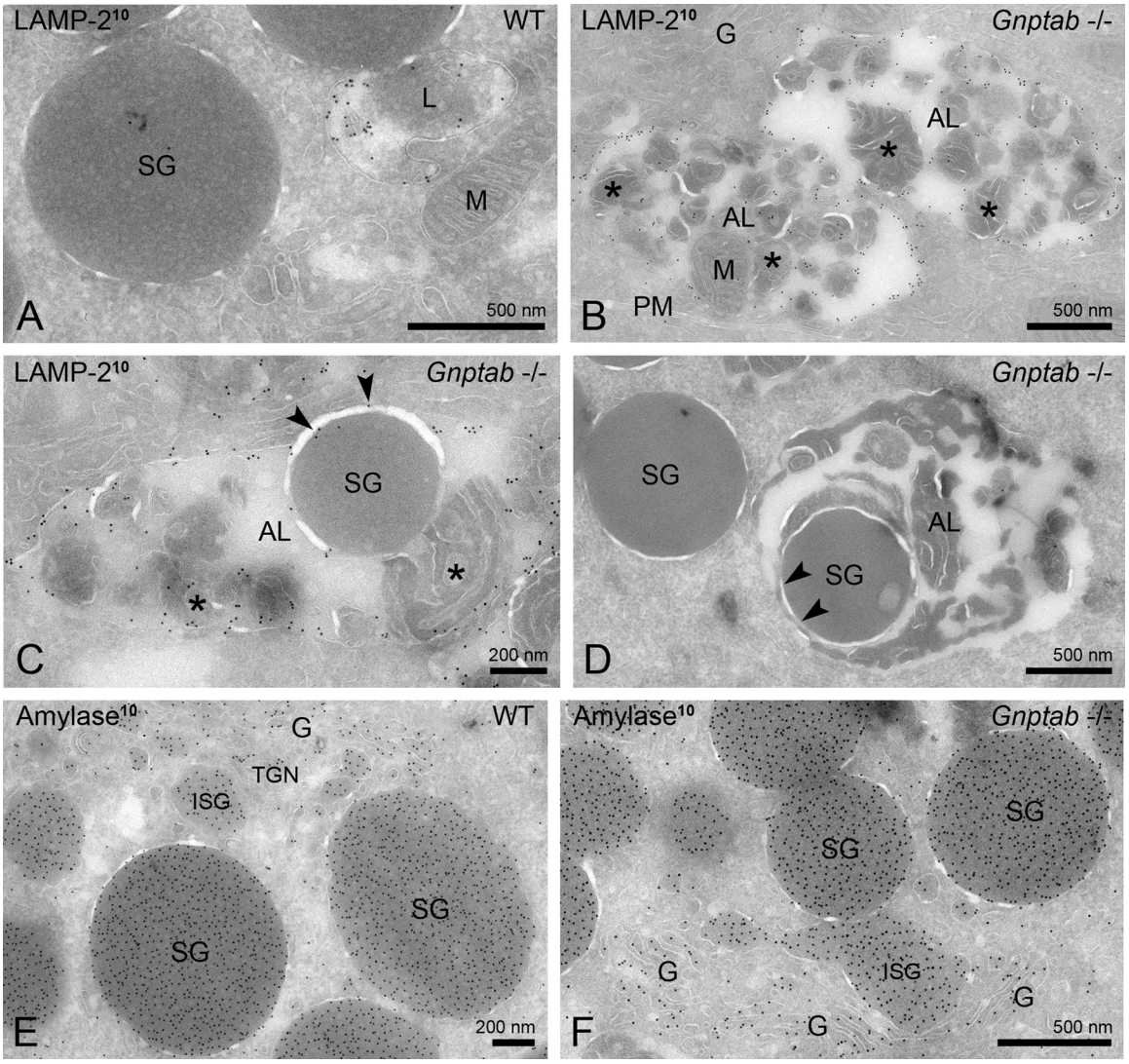

FIGURE 2: The acinar cells of *Gnptab* −/− mouse pancreas accumulate autolysosomes. (A–C) Ultrathin cryosections of wild-type and *Gnptab* −/− mouse exocrine pancreatic cells, immunogold labeled (10-nm gold particles) for LAMP-2. (A) Typical example of a LAMP-2 positive lysosome in wild-type (WT) cells. (B, C) *Gnptab* −/− pancreatic acinar cells accumulate numerous large LAMP-2 positive organelles that contain cytoplasmic material (asterisks), including (B) mitochondrial remnants and (C) secretory granules, which defines them as autolysosomes. The arrowheads in (C) show LAMP-2 labeling on the limiting membrane of the autolysosome, indicating that the secretory granule is enclosed within the autolysosome. (D) Another example of an autolysosome in *Gnptab* −/− pancreatic acinar cells that contains a secretory granule. The arrowheads indicate the membrane of the secretory granule, showing that the granule is inside the lumen of the autolysosome. (E, F) Immunogold labeling for amylase in (E) wild-type and (F) *Gnptab* −/− pancreas showing numerous secretory granules that appear similar in shape and density, albeit smaller in size in the *Gnptab* −/− cells. AL, autolysosome; G, Golgi apparatus; ISG, immature secretory granule; L, lysosome; M, mitochondrion; PM, plasma membrane; SG, secretory granule.

(Cao and Klionsky, 2007). The mTOR (kinase complex 1) is a central element in several sensing-signaling pathways that regulate cellular processes such as cell growth, nutrient import, protein synthesis, and autophagy (Pattingre *et al.*, 2008). It has been reported that, under various stress conditions, the inhibition of mTOR results in up-regulation of autophagy (Pattingre *et al.*, 2008; Jung *et al.*, 2010). We analyzed the activity of mTOR in the *Gnptab* −/− tissues by measuring the phosphorylation level of one of its downstream targets, the ribosomal kinase S6K (p70S6K). Our analysis showed that the level of Beclin-1 was slightly elevated in the *Gnptab* −/− exocrine glands (with the exception of the sublingual gland), whereas the phosphorylation of p70S6K was highly increased in these same tissues compared with wild-type animals (Figure 4A). These data indicate that, while the process of autophagy may be stimulated via the Beclin-1 pathway in the mutant cells, at the same time it is being inhibited by the activation of the mTOR pathway. Taken together, these observations suggest that macroautophagy is not strongly enhanced in these tissues. In accordance with this observation, evaluation of the occurrence of autophagosomes in EM sections of *Gnptab* −/− and wild-type pancreas did not reveal a significant increase in the number of these organelles in the mutant mice compared with wild-type (1.1 ± 0.2 autophagosomes per *Gnptab* −/− cell profile compared with 0.6 ± 0.1 for wild-type, $p = 0.11$) (Figure 4B). In contrast, the marked increase in the

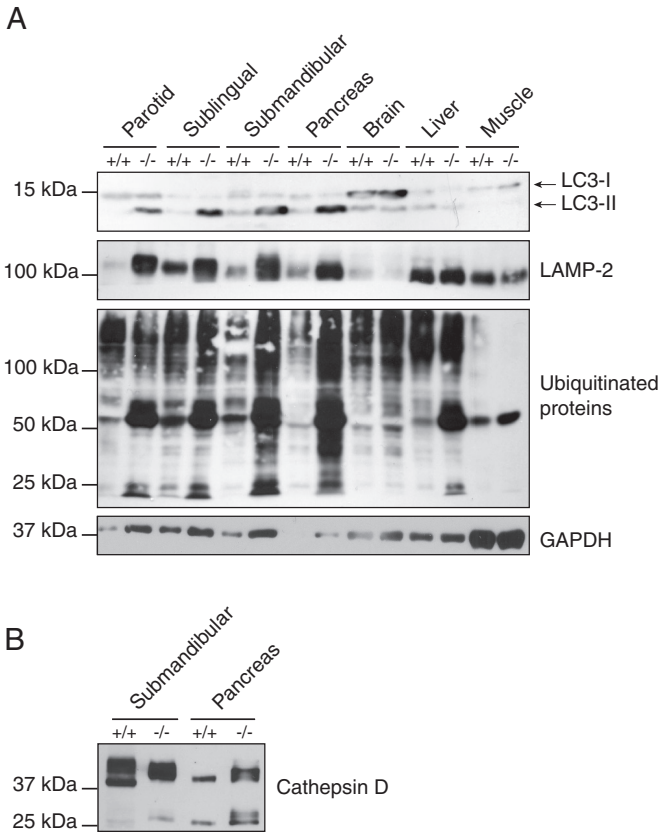

FIGURE 3: Steady-state levels of autophagy markers and lysosomal proteins in different tissues of wild-type and *Gnptab* −/− mice. (A) The levels of LAMP-2, LC3-II, and ubiquitinated proteins are greatly increased in the salivary and pancreatic glands of *Gnptab* −/− mice. Western blotting of the autophagy marker LC3 reveals that the level of the phosphatidylethanolamine-conjugated form of the protein, LC3-II, is highly increased in the parotid, sublingual, and submandibular salivary glands, as well as in the pancreas of the *Gnptab* −/− mice. An increase in the level of LAMP-2 is detected in the same organs, whereas the levels of both LC3-II and LAMP-2 are unchanged in the brain, liver, and muscle of the *Gnptab* −/− animals compared with wild-type levels. The immunoblot detection of ubiquitin shows that the levels of ubiquitinated proteins are modestly to strongly increased in the *Gnptab* −/− mouse salivary and pancreatic glands, while barely changed, if at all, in the brain and muscle of these mice compared with wild-type levels. A slight elevation of the level of ubiquitinated proteins is detected in the liver of the *Gnptab* −/− mice. The substrate of chaperone-mediated autophagy, GAPDH, is slightly increased in the exocrine secretory glands. (B) Cathepsin D levels as determined by Western blotting are similar in the *Gnptab* −/− submandibular salivary gland and slightly increased in the *Gnptab* −/− pancreas compared with wild-type levels. The mature enzyme is detected as a 39-kDa band, and partial processing to the heavy and light chain occurs in these tissues as shown by the presence of the 27-kDa band representing the heavy chain. Note that cathepsin D runs slightly slower in the *Gnptab* −/− tissues, which is due to differential processing of its N-linked glycans.

number of autolysosomes in *Gnptab* −/− acinar cells (26.2 ± 3.1 per cell profile vs. 1.5 ± 0.6 for the wild-type cells), as well as the decrease in the number of lysosomes (0.1 ± 0.1 in *Gnptab* −/− vs. 2.7 ± 0.5 in wild-type), attained statistical significance ($p < 0.01$).

It should be noted, however, that in the *Gnptab* −/− mucous-type secretory cells of the submandibular gland, engulfment of secretory granules by autolysosomes and direct fusion of secretory granules with these compartments (microautophagy and crinophagy, respectively) were often observed, suggesting that these processes may be stimulated even though the degree of macroautophagy appears not to be (Figure 1, E–G).

The acinar cells of *Gnptab* −/− mice exhibit decreased lysosomal degradative capacity

Our EM analysis showed that the acinar cells of the mutant mice submandibular and pancreatic glands accumulate autolysosomes that are filled with autophagic substrates, that is, secretory granule and mitochondrial remnants. By Western blot, we determined that this defect was accompanied by an increase in the level of LC3-II, which was also detected in the parotid and sublingual salivary glands of the mutant mice (Figure 3A). LC3-II is the phosphatidylethanolamine conjugated form of LC3-I that is formed upon recruitment of LC3-I from the cytosol onto the autophagosomal membrane during the process of autophagosome formation. After autophagosome closure, LC3-II on the surface of the autophagosome is released back into the cytosol, whereas the luminal pool of LC3-II is normally degraded after fusion of the autophagosomes with the lysosomes (Pattingre *et al.*, 2008). Because no obvious induction of macroautophagy was detected in the mutant glands, and because our EM analysis showed that the fusion of autophagosomes with lysosomes is not blocked in those tissues, the increase in the level of LC3-II strongly suggests a delay in its degradation within autolysosomes.

We also observed a striking increase in ubiquitinated proteins in the *Gnptab* −/− secretory glands compared with wild-type, especially in the mutant submandibular salivary gland and pancreas (Figure 3A). It was recently proposed that impaired progression of autophagy delays the delivery in ubiquitinated substrates to the proteasome (Korolchuk *et al.*, 2009), which could, at least in part, account for the increase of ubiquitinated proteins detected in the *Gnptab* −/− glands. In addition, because autophagy is a bulk degradation process, ubiquitinated proteins present in the cytosolic portions that are engulfed within forming autophagosomes would be expected to accumulate secondary to a defect of autolysosomal degradation. Finally, the *Gnptab* −/− glands displayed a slight increase in GAPDH, which is a substrate of chaperone-mediated autophagy, a process by which cytosolic proteins are directly translocated to the lysosomal lumen for degradation (Aniento *et al.*, 1993) (Figure 3A). These findings are all consistent with a defect in the degradative function of the lysosomes.

To determine whether this decrease in lysosomal degradative capacity might be accounted for by a reduction in the acid hydrolase content in lysosomes, we measured the activity of a number of lysosomal glycosidases (Table 1). All of these glycosidases are known to acquire the Man-6-P recognition marker (Sleat *et al.*, 2008), with the exception of β-glucocerebrosidase, which is targeted to the lysosomes by a Man-6-P–independent mechanism (Reczek *et al.*, 2007). The activities of α-mannosidase, β-galactosidase, β-mannosidase, and β-glucuronidase were modestly decreased in the pancreas of the *Gnptab* −/− mice (39–61% of wild-type levels) and in the submandibular salivary gland (28–89% of wild-type levels). The activity of α-galactosidase, however, was slightly elevated in both of these tissues of the mutant mice, while the activity of β-hexosaminidase was greatly increased in the pancreas (13.2-fold) but modestly decreased in the submandibular salivary gland. β-Hexosaminidase, in contrast to the other five glycosidases, has been shown to be associated with the lysosomal membrane (Yadao *et al.*, 1997; Magini *et al.*, 2008), as is β-glucocerebrosidase, whose activity was increased in both −/− pancreas and salivary gland (2.7- and 2.1-fold, respectively). However, it

	WT	–/–	Ratio –/–/WT		WT	–/–	Ratio –/–/WT
Pancreas				**Brain**			
α-Mannosidase	6.8 ± 2.0	3.9 ± 0.9*	0.57	α-Mannosidase	5.0 ± 0.6	7.6 ± 1.3*	1.52
β-Galactosidase	1.1 ± 0.2	0.7 ± 0.3*	0.61	β-Galactosidase	13.9 ± 4.4	8.5 ± 0.8*	0.61
α-Galactosidase	4.0 ± 0.7	6.0 ± 4.6	1.50	α-Galactosidase	8.2 ± 1.0	5.8 ± 0.4*	0.71
β-Mannosidase	66.6 ± 39.4	25.7 ± 9.6*	0.39	β-Mannosidase	3.5 ± 0.5	3.7 ± 0.6	1.05
β-Glucuronidase	3.9 ± 0.6	2.2 ± 1.2*	0.57	β-Glucuronidase	19.4 ± 2.4	26.4 ± 5.5*	1.36
β-Hexosaminidase	1.7 ± 0.5	22.8 ± 18.9*	13.2	β-Hexosaminidase	39.2 ± 5.2	55.6 ± 15.1*	1.42
β-Glucocerebrosidase	2.4 ± 0.7	6.5 ± 2.9*	2.70	β-Glucocerebrosidase	15.3 ± 6.4	26.4 ± 5.5*	1.73
Submandibular salivary gland				**Liver**			
α-Mannosidase	2 124.5 ± 1500.9	589.6 ± 604.1*	0.28	α-Mannosidase	14.4 ± 5.1	26.8 ± 7.3*	1.86
β-Galactosidase	48.8 ± 15.2	20.5 ± 13.7*	0.42	β-Galactosidase	16.5 ± 6.9	25.3 ± 6.4*	1.54
α-Galactosidase	21.7 ± 4.5	27.9 ± 13.8	1.28	α-Galactosidase	12.6 ± 2.0	18.1 ± 3.8*	1.44
β-Mannosidase	34.5 ± 13.6	24.6 ± 12.6	0.71	β-Mannosidase	12.5 ± 2.5	23.1 ± 5.2*	1.85
β-Glucuronidase	79.5 ± 22.2	70.5 ± 24.9	0.89	β-Glucuronidase	83.6 ± 20.4	102.4 ± 3.5	1.22
β-Hexosaminidase	117.6 ± 44.8	86.5 ± 36.6	0.74	β-Hexosaminidase	10.7 ± 3.3	33.7 ± 13.6*	3.16
β-Glucocerebrosidase	6.7 ± 1.3	14.0 ± 6.6*	2.08	β-Glucocerebrosidase	9.6 ± 3.4	14.2 ± 3.5*	1.47
Fibroblasts				**Muscle**			
α-Mannosidase	8.6 ± 2.8	1.3 ± 0.3*	0.15	α-Mannosidase	1.6 ± 0.5	2.9 ± 0.7*	1.79
β-Galactosidase	23.7 ± 9.0	2.0 ± 0.7*	0.08	β-Galactosidase	1.4 ± 0.5	1.1 ± 0.6	0.79
α-Galactosidase	ND	ND	ND	α-Galactosidase	1.3 ± 0.3	1.1 ± 0.6	0.84
β-Mannosidase	6.8 ± 2.0	1.1 ± 0.5*	0.16	β-Mannosidase	1.2 ± 0.4	1.8 ± 0.5	1.47
β-Glucuronidase	31.0 ± 10.5	7.8 ± 2.8*	0.25	β-Glucuronidase	10.2 ± 3.1	10.9 ± 2.8	1.07
β-Hexosaminidase	34.9 ± 9.2	4.1 ± 1.7*	0.12	β-Hexosaminidase	2.0 ± 0.7	2.1 ± 0.6	1.02
β-Glucocerebrosidase	24.1 ± 8.1	97.2 ± 29.8*	4.04	β-Glucocerebrosidase	1.6 ± 0.3	2.1 ± 0.5*	1.37

[a] Activities are expressed as nmol of methylumbellyferone released per mg protein per hour.
The values are the average ± SD, with n ≥ 6.
*p < 0.01; ND, not determined.

TABLE 1: Activity of acid hydrolases in wild-type (WT) and *Gnptab* –/– tissues and fibroblasts.[a]

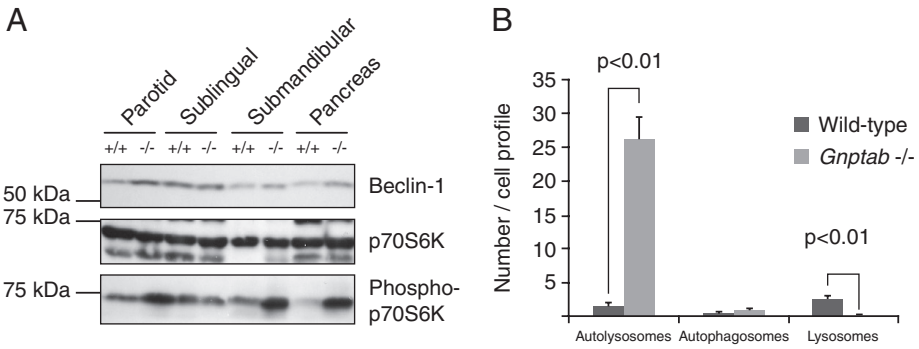

FIGURE 4: Analysis of mTOR activity and Beclin-1 levels in wild-type and *Gnptab* –/– exocrine tissues. (A) Western blot showing the levels of Beclin-1 and the mTOR target p70S6K (total and phosphorylated) in wild-type and *Gnptab* –/– salivary glands (parotid, sublingual, and submandibular) and pancreas. Equal amounts of protein were loaded, as reflected by the equal levels of total p70S6K in each lane. Note the very slight increase in the level of Beclin-1, and the more pronounced increase in the amount of phosphorylated p70S6K, in the –/– tissues compared with wild-type levels. (B) Graph representing the quantification of the number of autolysosomes, autophagosomes, and lysosomes present detected per cell profile by EM in the pancreas of wild-type and *Gnptab* –/– mice. The number of autolysosomes and lysosomes are significantly increased and decreased in *Gnptab* –/– ($p < 0.01$), respectively, whereas the number of autophagosomes is not changed.

is not clear at this point that the membrane association of β-hexosaminidase is related to the increased activity in the –/– pancreas, nor is it clear how this association would affect the targeting of this hydrolase.

We next determined the steady-state level of the protease cathepsin D in wild-type and *Gnptab* –/– submandibular salivary gland and pancreas by Western blotting. As shown in Figure 3B, the level of cathepsin D was similar to wild-type or even slightly increased in these *Gnptab* –/– tissues. In both tissues the major band was detected at ~39 kDa, which corresponds to the mature form of the enzyme. Some of the mature cathepsin D was processed into the heavy and light chains, as shown by the presence of the ~27-kDa heavy chain band. Cathepsin D had a slightly higher molecular weight in *Gnptab* –/– tissues, reflecting the differential processing of its N-linked glycans, which occurs in the absence of

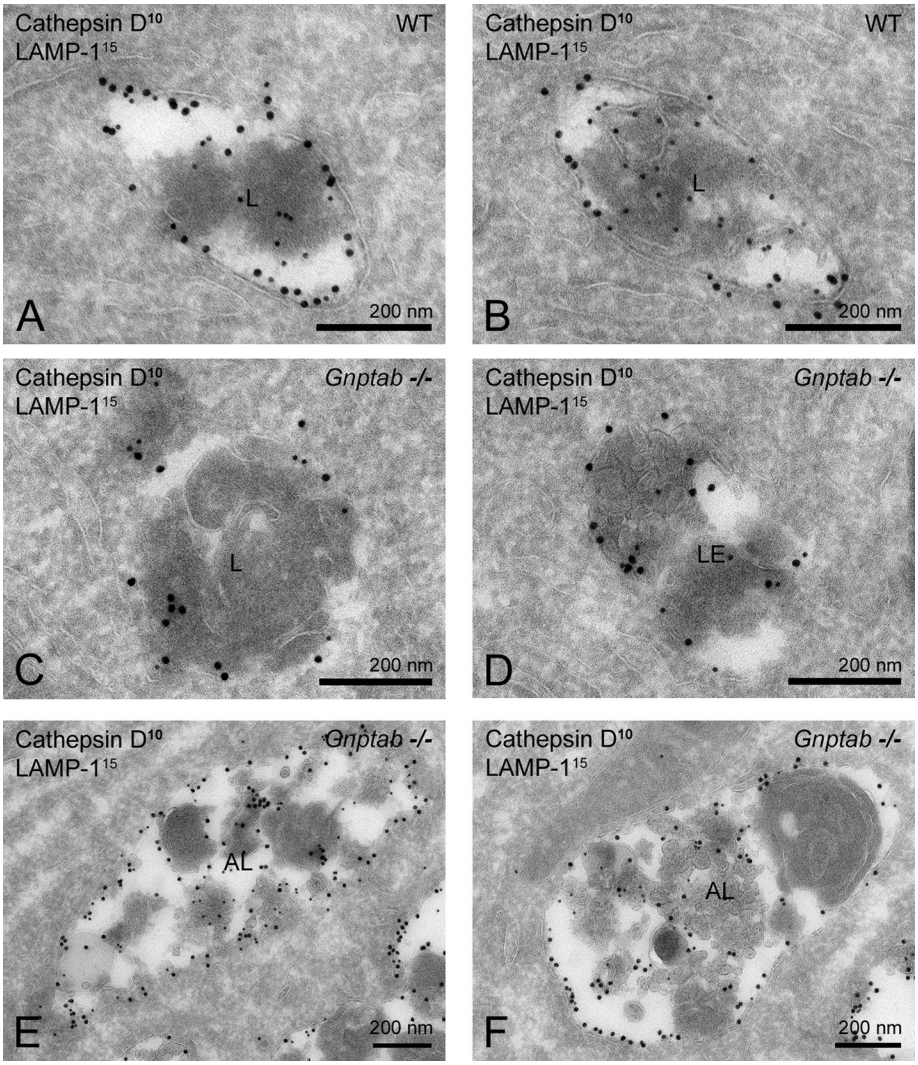

FIGURE 5: Lysosomes of *Gnptab* −/− pancreatic acinar cells contain reduced levels of cathepsin D. (A–F) Ultrathin cryosections of (A, B) wild-type and (C–F) *Gnptab* −/− pancreatic acinar cells immunogold labeled for cathepsin D (10-nm gold particles) and LAMP-1 (15 nm). (C, D) The endolysosomes in *Gnptab* −/− cells contain less cathepsin D compared with (A, B) wild-type cells. (E, F) Autolysosomes in *Gnptab* −/− pancreatic acinar cells contain low levels of cathepsin D. AL, autolysosome; L, lysosome; LE, late endosome.

phosphorylation of high-mannose–type sugar chains (Gelfman *et al.*, 2007).

The intracellular localization of cathepsin D in wild-type and *Gnptab* −/− pancreatic acinar cells was then evaluated by immuno-EM. Cathepsin D was readily detected in LAMP-1 positive late endosomes and lysosomes of cells of both types of mice (Figure 5, A–D) and in the autolysosomes of the *Gnptab* −/− acinar cells (Figure 5, E and F). By quantification, the endolysosomes of wild-type cells contained 11.3 ± 11.6 gold particles per compartment, whereas lower values (5.3 ± 4.6 gold particles per compartment) were measured in the *Gnptab* −/− endolysosomes ($p = 0.012$). Moreover, we observed that the average surface area of the individual late-endosomal and lysosomal compartments in *Gnptab* −/− cells was 1.4× larger compared with wild-type levels. Consequently, the density of cathepsin D labeling in the late endosomes and lysosomes of the *Gnptab* −/− pancreatic acinar cells was reduced to 37% of the labeling density in wild-type cells (53.3 ± 50.1 vs. 144.5 ± 103.8 gold particles per μm^2, respectively, $p = 7.35 \times 10^{-5}$), indicating decreased lysosomal targeting of cathepsin D in these cells.

The autolysosomes of the *Gnptab* −/− acinar cells contained low levels of cathepsin D labeling (Figure 5, E and F), consistent with dilution of the protease following fusion of the lysosomes with the autophagosomes. Because the total volume of autolysosomes in the *Gnptab* −/− acinar cells is so much larger than that of the lysosomes, a significant proportion of the total intracellular level of cathepsin D likely localizes to these compartments.

Loss of the Man-6-P signal does not affect tissues equally

Interestingly, in contrast to the exocrine glands of the *Gnptab* −/− mice, the liver, brain, and muscle of these mice contained normal levels of LAMP-2 and LC3-II (Figure 3A) and did not exhibit generalized vacuolization when examined by light or electron microscopy. In addition, the level of ubiquitinated proteins and GAPDH was unchanged in the muscle and brain of the *Gnptab* −/− mice compared with wild-type levels. Thus, at this level of analysis, the loss of the Man-6-P recognition system does not appear to impair the functioning of the autophagy or lysosomal system in these tissues. The liver of the mutant mice did exhibit a modest increase in the level of ubiquitinated proteins, although there was no accumulation of autolysosomes detected in this organ by EM (Supplemental Figure 1, A–D), and the levels of LC3-II and LAMP-2 were normal.

Direct enzyme assays revealed that the levels of the acid hydrolases in the brain and muscle of the *Gnptab* −/− mice were normal or even somewhat elevated compared with wild-type levels (1.0–1.8-fold) with the exception of β-galactosidase and α-galactosidase, whose activities were modestly decreased in the −/− brain by 39 and 29%, respectively (Table 1). The liver of the *Gnptab* −/− mice exhibited an increase in the activity of all the acid hydrolases measured (1.2–3.1-fold). To determine whether the acid hydrolases were actually in lysosomes, membrane fractions of brain and liver (from wild-type or *Gnptab* −/− mice) were fractionated on 18% self-forming Percoll density gradients as described previously (Boonen *et al.*, 2009), a technique that allows concentration of lysosomes in the densest fraction of the gradient (Figure 6), while the other organelles remain in the lighter fractions (Supplemental Figure 2). The analysis of the distribution of three different acid hydrolases (β-hexosaminidase, α-galactosidase, and α-mannosidase) revealed that a similar proportion of acid hydrolases localized to the dense-lysosome fraction in both organs, indicating that the lysosomes of *Gnptab* −/− brain and liver receive normal levels of acid hydrolases (Figure 6).

Skin fibroblasts of *Gnptab* −/− mice accumulate lysosomes and/or autolysosomes deficient in acid hydrolases

Because the presence of "inclusions" in fibroblasts of mucolipidosis type II patients is the hallmark of the disorder (also called

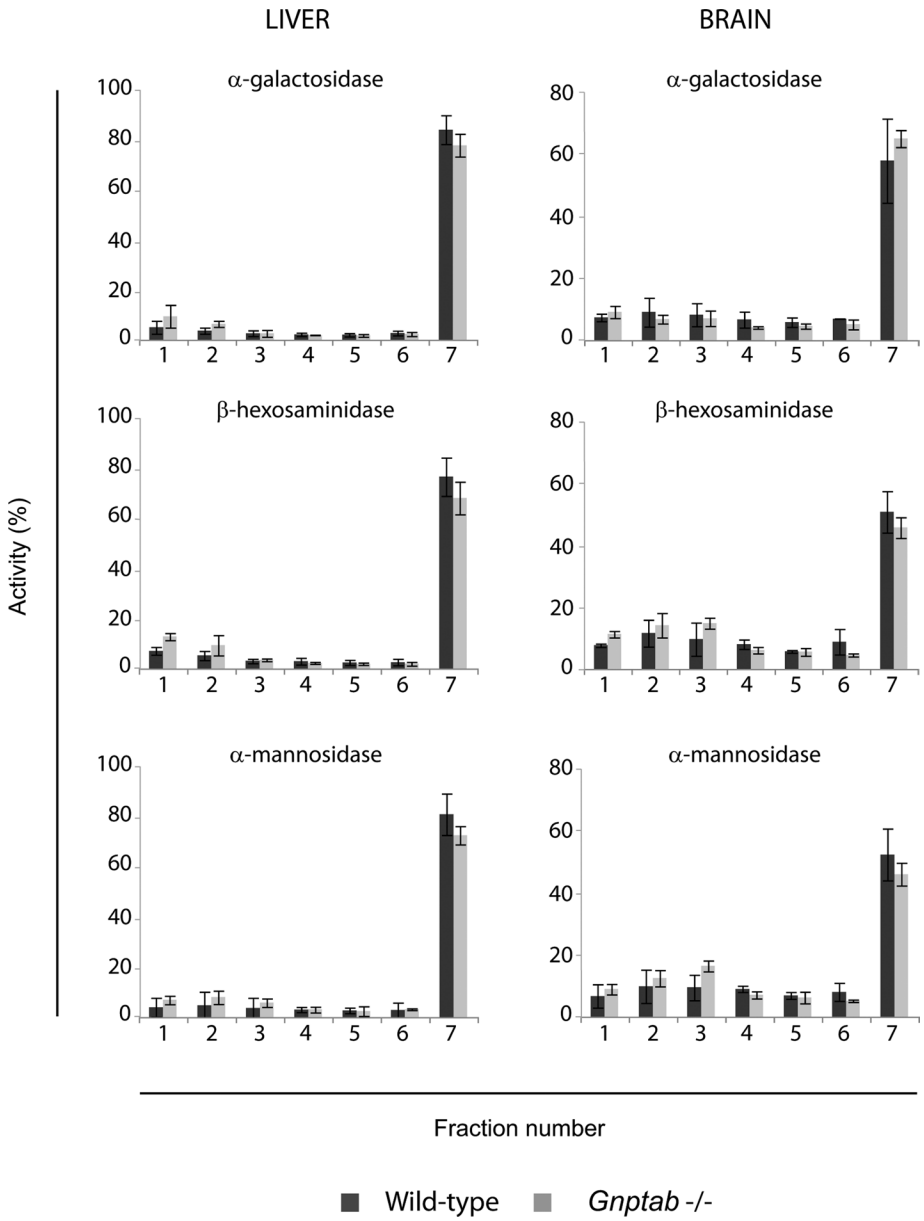

FIGURE 6: The subcellular distribution of acid hydrolases in the brain and liver of wild-type and *Gnptab* −/− mice is similar in a self-forming Percoll density gradient. Wild-type or *Gnptab* −/− liver and brain were homogenized in isotonic sucrose with a Potter-Elvehjem homogenizer and centrifuged at 1000 *g* to prepare a postnuclear supernatant (PNS). The PNS was subjected to centrifugation at 35,000 rpm in a 50Ti rotor for 40 min at 4°C to obtain a membrane fraction which was resuspended in isotonic sucrose and loaded on top of an 18% Percoll solution. Self-forming gradients were generated by centrifugation at 25,000 rpm in a SW55Ti rotor for 40 min at 4°C. Seven fractions were collected from the top (low density) to the bottom (densest fraction) and acid hydrolase content was determined by enzyme assays. Graphs represent the distribution of α-galactosidase, β-hexosaminidase, and α-mannosidase in wild-type (n = 3) or *Gnptab* −/− (n = 3) liver and brain, expressed as a percentage of the total activity recovered in each fraction.

I-cell disease for inclusion-cell disease), we were surprised that we did not detect morphological alterations in the fibrocytes and fibroblasts examined during the histologic survey of the *Gnptab* −/− mouse tissues (Vogel *et al.*, 2009). Subsequently, we became aware of a 1975 publication by Aula *et al.* reporting that fibroblasts in tissues from a human mucolipidosis II fetus had detectable inclusions when the samples were embedded in epoxy, but not in paraffin, the method used for our prior histologic analysis (Aula *et al.*, 1975). Therefore we isolated skin fibroblasts from the *Gnptab* −/− mice and examined them by immuno-EM. Figure 7A shows strong labeling of the lysosomal protease cathepsin D in skin fibroblasts of wild-type mice. Lysosomes with a diameter of 400–600 nm were detected, containing lamellar material as well as small internal membrane vesicles. By contrast, the fibroblasts derived from the *Gnptab* −/− mice had increased numbers of lysosomes that contained very low levels of cathepsin D (Figure 7B) but were positive for the lysosomal membrane protein LAMP-2 (Figure 7, C and D). This deficiency of cathepsin D reflects the known hypersecretion of this protease by this cell type (Lee *et al.*, 2007). The lysosomes were enlarged (up to ~1.5 μm in diameter), filled with dense amorphous material, and occupied much of the cytoplasm (Figure 7C). Mitochondrial remnants were occasionally detected within these compartments, indicating that they had received material via the autophagic pathway and had become autolysosomes (Figure 7D). The difference in size and composition of these enlarged lysosomes and autolysosomes (~1.5 μm, mainly amorphous content) compared with their counterparts in the exocrine tissues (up to 4 μm with numerous organelle remnants) might explain why the latter gave rise to vacuolization that is readily detectable in paraffin sections while the other did not.

Measurements of the activity of five lysosomal hydrolases revealed extremely low levels in the *Gnptab* −/− fibroblasts (8–25% of wild-type levels), whereas the activity of β-glucocerebrosidase was increased fourfold over wild-type levels (Table 1). The *Gnptab* −/− fibroblasts also showed increased levels of LAMP-2 and LC3-II, as well as a slight increase in ubiquitinated proteins compared with wild-type fibroblasts (Figure 8, A and B). No difference in the level of GAPDH was detected, suggesting that the process of chaperone-mediated autophagy was not impaired in those cells. As in the exocrine glands, the level of phosphorylation of the mTOR target p70S6K was elevated in the *Gnptab* −/− fibroblasts compared with wild-type levels, indicating inhibition rather than activation of the macroautophagy pathway (Figure 8C). The cellular level of Beclin-1 was unchanged (Figure 8C).

These findings show that the *Gnptab* −/− fibroblasts accumulate enlarged lysosomes and/or autolysosomes, most likely secondary to the severe depletion of acid hydrolases that impairs the degradative function of the lysosomes and autolysosomes. A similar decrease in acid hydrolase content was reported in fibroblasts isolated from mucolipidosis type II patients and from a

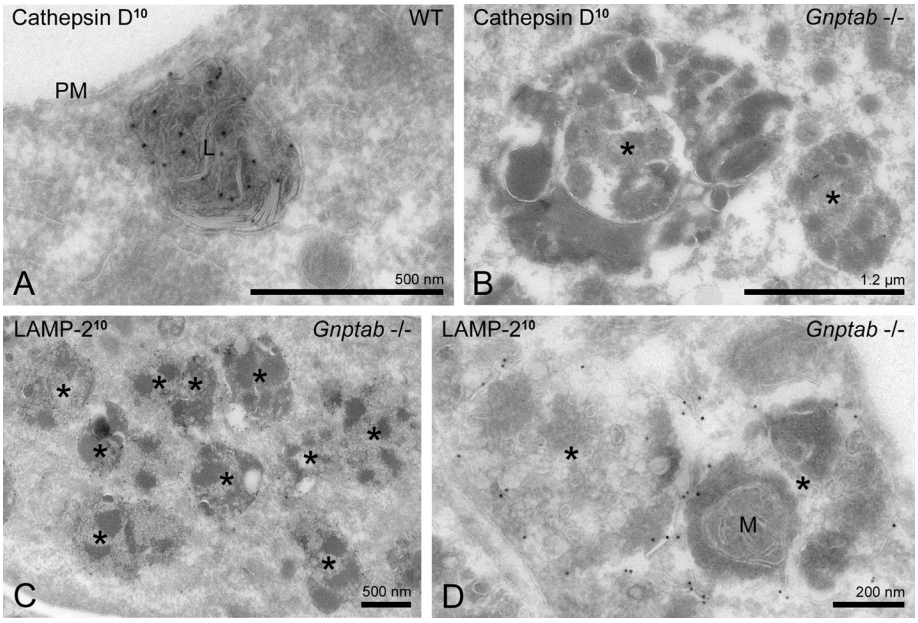

FIGURE 7: *Gnptab* −/− mouse skin fibroblasts accumulate enlarged lysosomes and/or autolysosomes. (A) Electron micrograph of a typical lysosome in wild-type mouse skin fibroblasts immunogold labeled (10-nm gold particles) for cathepsin D. (B–D) Electron micrographs showing the accumulation of enlarged lysosomes and/or autolysosomes (asterisks) in *Gnptab* −/− mouse skin fibroblasts, recognized by their dense heterogeneous content, the occasional presence of (D) mitochondrial remnants, and (C, D) the detection of LAMP-2 in their membrane. (B) The enlarged lysosomes and autolysosomes contain low levels of cathepsin D. M, mitochondrion; PM, plasma membrane; *, swollen lysosome or autolysosome.

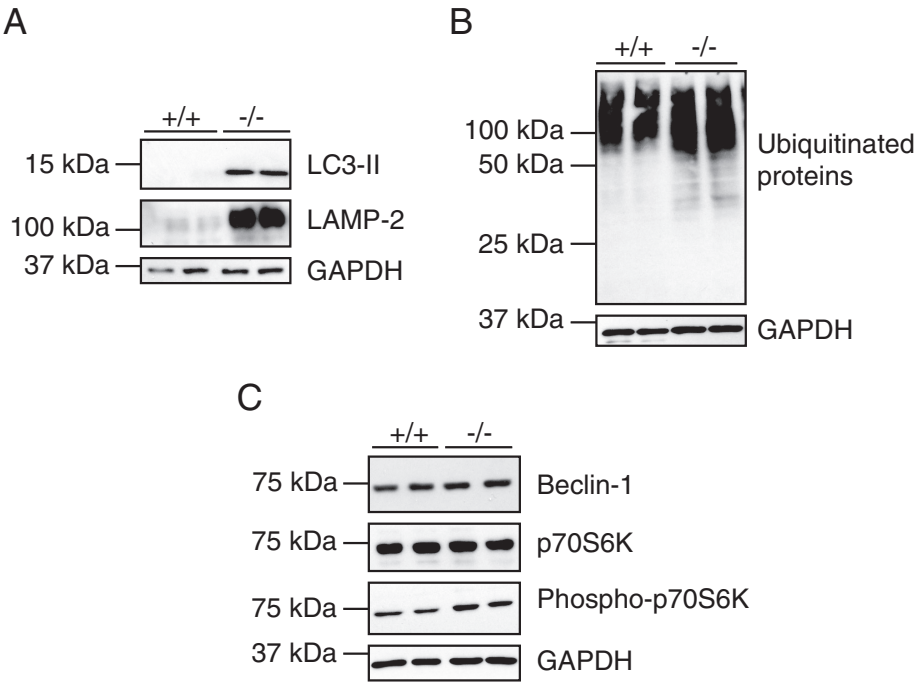

FIGURE 8: The level of LC3-II is elevated in *Gnptab* −/− mouse skin fibroblasts, while stimulation of macroautophagy via the Beclin-1 or mTOR pathway is not detected. (A, B) Immunoblots showing the increased levels of (A) LC3-II and LAMP-2 and (B) ubiquitinated proteins in *Gnptab* −/− mouse skin fibroblasts over wild-type levels. (Two independent cell lysates are shown for each genotype, indicated as +/+ and −/− for wild-type and *Gnptab* −/− mice, respectively.) (C) Detection by Western blotting of Beclin-1, whose levels are unchanged between +/+ and −/− cells, and of the mTOR target p70S6K, which is slightly more phosphorylated in the −/− fibroblasts compared with wild-type cells. (A–C) The level of GAPDH is similar in +/+ and −/− cells.

Gnptab knock-in mouse model of mucolipidosis type II (Kornfeld and Sly, 2000; Kollmann *et al.*, 2010). Moreover, Otomo *et al.* recently showed that fibroblasts of patients with mucolipidosis II accumulate autolysosomes that can account for the inclusions initially observed by light microscopy (Leroy and Demars, 1967; Otomo *et al.*, 2009).

DISCUSSION

We previously reported that acinar cells of the exocrine glands of *Gnptab* −/− (MLII) mice exhibit extensive vacuolization when examined by light microscopy (Gelfman *et al.*, 2007; Vogel *et al.*, 2009). These morphological abnormalities are similar to those described in the exocrine pancreas, salivary glands, and gastric chief cells of several MLII patients (Elleder and Martin, 1998). On the basis of our analysis of the acinar cells of the salivary and pancreatic glands of *Gnptab* −/− mice, we now demonstrate that the vacuolization represents the accumulation of autolysosomes in the mucous and serous cells of these organs. Our data show that these autolysosomes are defective in degradative capacity, accounting for their striking accumulation. Yet the involved exocrine glands retain substantial amounts of acid hydrolases despite the loss of the Man-6-P signal. This finding is in contrast to fibroblasts which have similar morphological alterations but extremely low levels of acid hydrolases due to massive hypersecretion of these enzymes.

These observations can be explained by considering the unique role of the Man-6-P sorting pathway in regulated secretory cells compared with other cell types (i.e., the fibroblasts). In fibroblasts, the newly synthesized acid hydrolases are packaged at the TGN into clathrin-coated carriers by a Man-6-P–dependent mechanism and transported to the lysosomes (Figure 9C). When the synthesis of the Man-6-P signal is defective, as occurs in *Gnptab* −/− mice, the acid hydrolases are hypersecreted via the constitutive secretory pathway, resulting in very low cellular levels of the hydrolases (Figure 9D) (Lee *et al.*, 2007). In the regulated secretory cells (Figure 9A), a portion of the newly synthesized acid hydrolases are similarly packaged into clathrin-coated carriers at the TGN and transported to lysosomes. However, studies of pancreatic beta-cells have shown that the majority of the hydrolases escape entry into the clathrin-coated carriers and instead enter immature secretory granules (ISGs) that bud from the TGN (Kuliawat and Arvan, 1994). During granule maturation, the Man-6-P–containing acid

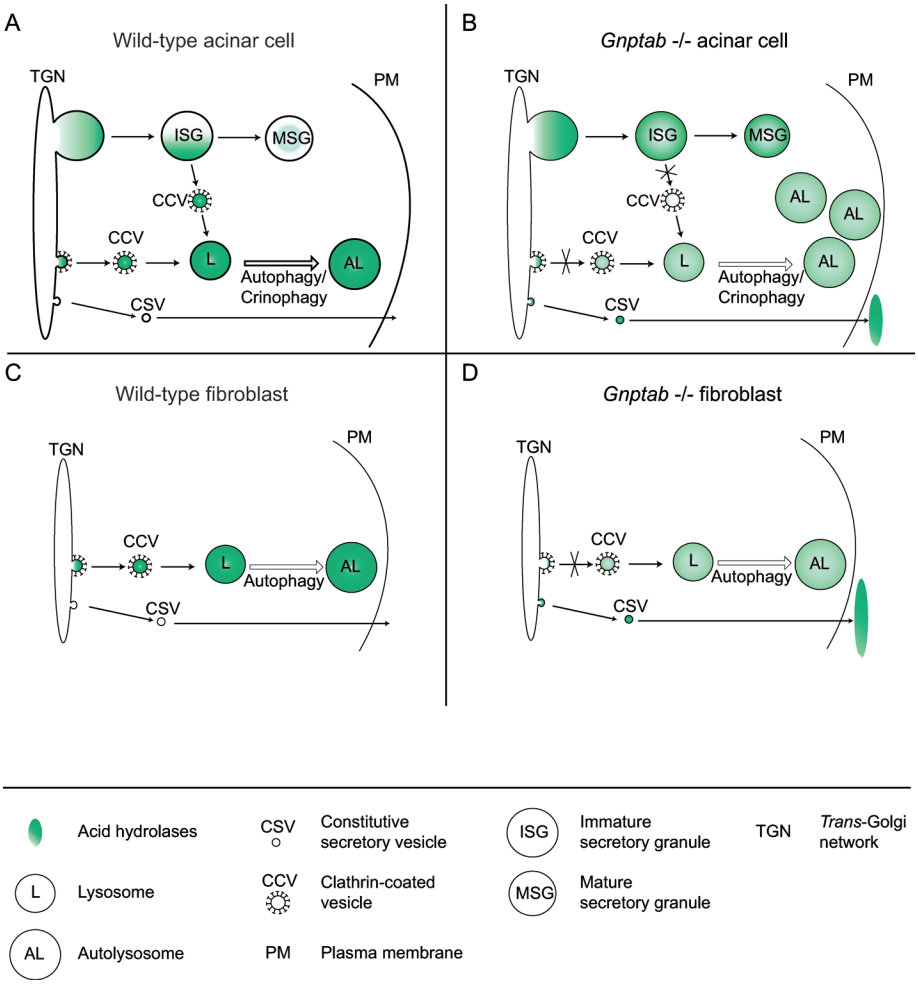

FIGURE 9: Model for the consequences of the lack of the Man-6-P signal on the trafficking of acid hydrolases in fibroblasts and secretory cell types (salivary and pancreatic gland acinar cells). (A) In secretory cell types, acid hydrolases can reach the lysosomes by two pathways: direct sorting from the TGN, or retrieval from the ISGs that had incorporated a portion of the newly synthesized hydrolases while budding off the TGN. Both processes involve packaging of the hydrolases in CCVs by a Man-6-P–dependent mechanism. (B) In the absence of the Man-6-P signal (*Gnptab* −/− cells), the hydrolases either undergo constitutive secretion or are trapped within mature secretory granules due to the lack of retrieval from the ISGs. As a result, lysosomes (L) have low levels of acid hydrolases. The accumulation of autolysosomes (AL) in the salivary glands and pancreas of the *Gnptab* −/− mice is the consequence of the resulting defective lysosomal degradative capacity. (C) In normal fibroblasts, acid hydrolases are packaged into clathrin-coated transport carriers at the TGN and targeted to lysosomes (L) in a Man-6-P–dependent manner. (D) The loss of the Man-6-P signal in *Gnptab* −/− fibroblasts, and the subsequent lack of recognition of the hydrolases at the TGN, results in their hypersecretion via the constitutive secretory pathway. Consequently, lysosomes (L) and autolysosomes (AL) with low acid hydrolase content and poor degradative capacity accumulate.

hydrolases are then removed by a mechanism involving binding to Man-6-P receptors (MPRs) and incorporation into AP-1 and syntaxin-6-positive clathrin-coated vesicles (CCVs) that bud from the ISGs and transport their cargo to endolysosomes (Tooze and Tooze, 1986; Kuliawat *et al.*, 1997; Klumperman *et al.*, 1998; Dittié *et al.*, 1999). This process provides an "exit site" for acid hydrolases that enter the regulated secretory pathway, allowing retrieval to lysosomes. The inability to synthesize the Man-6-P marker in the *Gnptab* −/− mice would have several consequences in these cells (Figure 9B). At the TGN, the newly synthesized acid hydrolases would be poorly sorted into CCVs due to their inability to bind MPRs, which would result in increased secretion via the constitutive secretory pathway and even greater packaging of the hydrolases into ISGs. Most important, once the hydrolases enter the ISGs, they would not be retrieved by the Man-6-P–dependent system. This hypothesis is supported by the observations of Kuliawat *et al.*, who reported that the loss of one of the two MPRs in mice, the cation-dependent MPR, resulted in a nearly fourfold increase in the presence of the precursor form of cathepsin B in the regulated secretory pathway of pancreatic beta-cells (Kuliawat *et al.*, 1997). The lack of binding of acid hydrolases to both of the MPRs in *Gnptab* −/− mice exocrine cells would be expected to impair the sorting and retrieval of the acid hydrolases to lysosomes even more. As a result, their lysosomes would be deficient in acid hydrolases and unable to efficiently degrade material derived from the endocytic and autophagic pathways. The finding that the cathepsin D content of the pancreatic acinar cell lysosomes of *Gnptab* −/− mice is decreased to 37% of the wild-type levels whereas the total cellular content of this protease is normal or even increased is consistent with this model.

In addition, the modest decrease in the intracellular levels of several other acid hydrolases suggests their increased secretion by the *Gnptab* −/− acinar cells, either via the constitutive secretory pathway and/or as the result of secretory granule fusion with the plasma membrane followed by release of their contents. It should be noted that the extent of this secretion could be underestimated in our assay. The steady-state level of the acid hydrolases in the acinar cells is determined by the rate of synthesis, the extent of secretion, and their half-life. Sardiello *et al.* reported that acid hydrolase synthesis is up-regulated in fibroblasts from patients with several forms of lysosomal storage diseases (Sardiello *et al.*, 2009). If acid hydrolase synthesis is increased in the acinar cells of the *Gnptab* −/− mice, this could help maintain the intracellular levels of some acid hydrolases in the face of significant hypersecretion of these enzymes. Nevertheless the issue of entrapment in secretory granules would remain. Finally, because we only assayed for a limited number of acid hydrolases, we cannot exclude the possibility, although unlikely, that one particular acid hydrolase (out of the total 60 enzymes that reside in lysosomes) might be dramatically reduced in the lysosomes, leading to the impaired degradative capacity of these compartments.

Unfortunately we were unable to formally demonstrate the missorting of the acid hydrolases into mature secretory granules of the mutant cells. By immuno-EM using cathepsin D antibodies, we only observed background labeling of the secretory granules of wild-type and mutant pancreatic acinar cells. In addition, homogenization and subcellular fractionation of the *Gnptab* −/− pancreas

resulted in extensive autolysosome disruption, which made it impossible to determine whether the secretory granules in the mutant pancreas contained increased amounts of acid hydrolases. Meister *et al.* recently reported this same problem with pancreatic tissue of cation-independent MPR–deficient mice (Meister *et al.*, 2010). Similar to our work, these authors described the formation of large cytoplasmic vacuoles in the pancreas of those mice, although much less severe than in the *Gnptab* −/− mice (Gelfman *et al.*, 2007).

We did not detect convincing evidence for macroautophagy activation in the exocrine glands of the *Gnptab* −/− mice (3–4-mo-old mice), based on evaluation of Beclin-1 levels and activity of mTOR. However, we cannot rule out the possibility that stimulation of macroautophagy may have contributed to pathological development at an earlier stage of the process. In addition, the numerous profiles of ongoing crinophagy and microautophagy observed in the mutant salivary glands raise the possibility that these processes may be stimulated, perhaps representing an attempt to dispose of secretory granules that have been damaged by their content of acid hydrolases. This activation could contribute to the accumulation of autolysosomes. In the *Gnptab* −/− pancreas, the accumulation of autolysosomes was accompanied by a decrease in the number of lysosomes. These data are consistent with the recent report that inhibition of autolysosomal protein degradation with protease inhibitors abrogates lysosome reformation, leading to the accumulation of enlarged and long-lived autolysosomes (Yu *et al.*, 2010). The accumulation of autolysosomes in our MLII mouse also points out an important difference compared with other lysosomal storage disorders with autophagy defects, including multiple sulfatase deficiency and mucopolysaccharidosis IIIA. Studies of mouse models of these disorders revealed that the affected cells exhibit an accumulation of autophagosomes, rather than autolysosomes, resulting from a defect in the fusion of the autophagosomes with lysosomes (Settembre *et al.*, 2008; Fraldi *et al.*, 2010). By contrast, the defect in the *Gnptab* −/− mice appears to be the failure to dispose of the engulfed material by lysosomes and autolysosomes deficient for critical lysosomal hydrolases.

Our data support previous reports that the requirement for the Man-6-P–dependent sorting pathway varies substantially among cell types. At one extreme, fibroblasts (cells of mesenchymal origin) are highly dependent on the Man-6-P pathway for efficient acid hydrolase sorting and lysosomal function. Our findings now demonstrate that the lysosomal function of the exocrine secretory cells is also highly dependent on the Man-6-P pathway. It is of note that exocrine secretory cells and organs, including the pancreas, appear to have a relatively high basal level of autophagy compared with other tissues (Mizushima *et al.*, 2004). This might explain why the autolysosomes detected in the exocrine cells of the *Gnptab* −/− mice were generally more prevalent than observed in fibroblasts and often filled with easily recognizable remnants of material derived from macro-, micro-, or crinophagy. At the other extreme, the liver, brain, and muscle of the *Gnptab* −/− mice have normal or even elevated levels of acid hydrolases that are correctly localized within lysosomes, despite the loss of the Man-6-P signal, and do not exhibit any obvious morphological alterations. These findings are in agreement with those previously reported for postmortem samples obtained from patients with MLII (Kenyon *et al.*, 1973; Martin *et al.*, 1975, 1984; Nagashima *et al.*, 1977; Owada and Neufeld, 1982; Waheed *et al.*, 1982). The liver, which is known to have a high endocytosis capacity, had an increased level of all the measured acid hydrolases, which could reflect their capture from the plasma where the levels are extremely elevated in the mutant mice (Gelfman *et al.*, 2007). However, while endocytosis might contribute to the normal or elevated levels of acid hydrolases in the brain and muscle, a more likely explanation is that these tissues utilize an intracellular Man-6-P–independent targeting pathway(s). This is consistent with previous studies demonstrating the existence of a Man-6-P–independent intracellular sorting pathway for cathepsin D in MLII lymphoblasts and thymocytes isolated from mice deficient in both Man-6-P receptors (Glickman and Kornfeld, 1993; Glickman *et al.*, 1996; Dittmer *et al.*, 1999). A major goal of future work will be to identify the molecular basis of the Man-6-P–independent pathway(s).

MATERIALS AND METHODS

Materials

Chemicals, including fluorogenic substrates for acid hydrolase enzyme assays, were obtained from Sigma Aldrich (St. Louis, MO) unless otherwise specified. Mouse anti-ubiquitin antibody and rabbit anti–Beclin-1, p70S6K, and phospho-p70S6K (Thr389) antibodies were purchased from Cell Signaling Technology (Danvers, MA). Rabbit anti-LC3 and mouse anti-GAPDH antibodies were obtained from Novus Biologicals (Littleton, CO) and Sigma Aldrich, respectively, and both rat anti–LAMP-1 and rat anti–LAMP-2 antibodies from Developmental Studies Hybridoma Bank (Iowa City, IA). Goat anti-amylase antibody was purchased from Santa Cruz Biotechnology (Santa Cruz, CA) and rabbit anti-amylase (AMY2B) from Proteintech Europe (Manchester, UK). The rabbit anti–cathepsin D used for Western blots was produced in our laboratory. Cathepsin D was detected in immuno-EM with a rabbit anti–cathepsin D antibody that was a generous gift from M. Koike (Juntendo University Graduate School of Medicine, Tokyo, Japan). Horseradish peroxidase (HRP)–coupled secondary antibodies were purchased from GE Healthcare (Piscataway, NJ). For immuno-EM, rabbit anti–rat immunoglobulin (Ig)G polyclonal antibody (DAKO, Heverlee, Belgium) was used as a bridging step between rat monoclonal antibody (mAb) and protein A-gold (Cell Microscopy Center, UMC Utrecht, the Netherlands). Cellgro Alpha-Minimum Essential Media and penicillin/streptomycin were obtained from Fisher Scientific (Pittsburgh, PA) and fetal calf serum (FCS) from ISC BioExpress (Kaysville, UT). The *Gnptab* −/− mice were described previously (Gelfman *et al.*, 2007).

Enzyme assays

Mouse skin fibroblasts were isolated from wild-type and *Gnptab* −/− mouse ears and maintained in α-MEM medium containing 20% FCS, 100 µg/ml penicillin, and 100 U/ml streptomycin. Organs were collected from 3–4-mo-old mice after perfusion through the heart with phosphate-buffered saline (PBS) (137 mM NaCl, 2.7 mM KCl, 10 mM Na_2HPO_4, 1.76 mM KH_2PO_4, pH 7.5). Tissues or confluent cells in culture were suspended in PBS containing 1% Triton X-100 and a mixture of protease inhibitors (complete mini protease inhibitor tablets; Roche, Penzberg, Germany) for 15 min on ice and then sonicated and centrifuged for 15 min at 13,000 *g*. Lysosomal hydrolase activities were determined in the supernatants by fluorometric enzyme assays as described (Lee *et al.*, 2007). Briefly, the samples were incubated with either 1 mM (tissue samples) or 5 mM (cultured fibroblasts lysates) of 4-methylumbelliferyl–coupled specific substrates in a 50-mM citrate buffer containing 0.5% Triton X-100 (pH 4.5) at 37°C, except for the β-glucocerebrosidase assay that was performed in a buffer containing 0.1 M sodium citrate, 0.2 M Na_2HPO_4, 0.2% TX-100, and 0.25% sodium taurocholate, pH 5.2. Reactions were stopped by addition of 0.1 M glycine-NaOH solution (pH 10.3) and the fluorescence was read at 495 nm. Activities were expressed as nanomoles of hydrolyzed methylumbelliferone per milligram protein and per hour.

Percoll density gradients

Wild-type and *Gnptab* −/− mice that were 2–3 mo of age were anesthetized and subsequently perfused with PBS to remove blood from their organs. The brains and livers of these mice were removed and fractionated on an 18% self-forming Percoll density gradient as described previously (Boonen *et al.*, 2009). Briefly, a membrane fraction was prepared, loaded on top of an 18% Percoll solution (18% [vol/vol] Percoll [Pharmacia, Uppsala, Sweden], 0.25 M sucrose, 2 mM EDTA, and 10 mM Tris/HCl [pH 7.4]) and centrifuged at 25,000 rpm in a Beckman SW55Ti rotor for 40 min at 4°C. Seven fractions were collected from the top of the gradient. The distribution of three different lysosomal hydrolases was determined by enzyme assays as described earlier.

Western blotting

Identical amounts of wild-type or *Gnptab* −/− protein samples (lysed in PBS containing 1% Triton X-100 and protease inhibitors as described earlier) were resolved on polyacrylamide gels and transferred onto polyvinylidene fluoride membranes (Millipore, Billerica, MA), which then were blocked in 10% fat-free milk in PBS/Tween 0.1% for 30 min at room temperature (RT) prior to incubation overnight at 4°C with primary antibodies diluted in PBS/Tween 0.1% containing 0.2% fat-free milk. After washing with PBS/Tween 0.1%, blots were incubated for 45 min at RT with HRP-coupled secondary antibodies diluted in PBS/Tween 0.1% containing 0.2% fat-free milk and washed. Immunoreactive bands were revealed by chemiluminescence (ECL Amersham, Piscataway, NJ).

EM

Wild-type and *Gnptab* −/− mice at 1.5–2 mo of age were sedated and perfused via the heart with either 2% wt/vol paraformaldehyde (PFA) in 0.1 M phosphate buffer (PB) pH 7.4 or 2% wt/vol PFA, 0.2% wt/vol glutaraldehyde (GA, from Polysciences Europe GmbH, Eppelheim, Germany) in 0.1 M PB, pH 7.4. Following the perfusion fixation with 2% PFA, the tissues were removed and immediately immersed in 4% wt/vol PFA in 0.1 M PB and kept overnight at 4°C. In case of the perfusion fixation with 2% PFA, 0.2% GA, the tissues of interest were divided into two halves and either immersed in the same fixative, kept overnight at 4°C, and processed for cryosectioning or immersed in 2% wt/vol PFA, 2.5% wt/vol GA in Na-cacodylate buffer (Karnovsky fixative) for 2 h at RT. Subsequently, the Karnovsky fixative was replaced for 0.1 M Na-cacodylate buffer, pH 7.4. Prior to Epon embedding, the tissues were postfixed with 1% wt/vol OsO_4, 1.5% wt/vol $K_3Fe(III)(CN)_6$ in 0.065 M Na-cacodylate for 2 h at 4°C. Subsequently the tissues were stained with 0.5% uranyl acetate for 1 h at 4°C, dehydrated with ethanol, and embedded in Epon. Ultrathin sections were stained with uranyl acetate and lead citrate.

For cryosectioning and immuno-EM, the fixed tissues were further processed as described (Slot and Geuze, 2007). In short, the tissues were cut into small blocks, rinsed with PBS and PBS containing 0.02 M glycine, and embedded in 12% gelatin. The blocks were incubated overnight in 2.3 M sucrose at 4°C, mounted on metal pins, and frozen in liquid nitrogen. Ultrathin cryosectioning was performed at −120°C in a Leica UCT-FCS ultracryomicrotome (Leica Microsystems, Vienna, Austria). The sections were transferred to copper grids by pickup with a 1:1 mixture of 2.3 M sucrose in PBS and 2% wt/vol methyl cellulose. For immunogold labeling, the grids were incubated first on 2% gelatin/PBS at 37°C, blocked with 0.02 M glycine/PBS and 1% bovine serum albumin/PBS, and subsequently incubated with primary antibodies followed by protein A-gold. The sections were contrasted with 2% uranyl acetate/oxalate, pH 7, followed by 0.4% uranyl acetate pH 4 and 1.8% methyl cellulose (Slot and Geuze, 2007).

Mouse skin fibroblasts were fixed by addition of an equal volume of 4% wt/vol PFA in 0.1 M PB to the culture medium. After ~10 min, the fixative was replaced for 4% wt/vol PFA in 0.1 M PB for at least 2 h at RT and the cells were processed for cryosectioning and immunogold labeling.

All sections were analyzed in a JEOL 1200 EX (Tokyo, Japan) electron microscope at 60 or 80 kV for Epon or cryosections, respectively. Quantification of the number of autophagosomes, autolysosomes, and lysosomes was performed in ultrathin cryosections of wild-type and *Gnptab* −/− pancreas labeled for LAMP-2. Values are average numbers per cell profile ± SE of the mean. Autophagosomes were defined as compartments containing cytoplasmic material but that were devoid of LAMP-2 labeling. Autolysosomes were distinguished by the presence of undegraded cytoplasmic material and the presence of LAMP-2 on their limiting membrane, whereas lysosomes were defined as LAMP-2–positive compartments with homogeneous content that occasionally contained visible internal membrane sheets. In total, 15 cell profiles from two grids of wild-type or *Gnptab* −/− pancreatic acinar cells were assessed for the presence of lysosomes and autolysosomes and 30 cell profiles for the presence of autophagosomes. Quantification of the cathepsin D labeling in late endosomes and lysosomes of wild-type and *Gnptab* −/− pancreatic acinar cells was performed by random screening of LAMP-1 and cathepsin D double-labeled sections. Late endosomes and lysosomes were defined as LAMP-1–positive compartments with a diameter size >200 nm that were devoid of undegraded autophagic material. The number of gold particles representing cathepsin D was scored per compartment. In total, 29 endolysosomal compartments were assessed in both wild-type and *Gnptab* −/− cells, out of which the average cathepsin D labeling level was determined; ± values are standard deviations. The surface of the late endosomes and lysosomes was measured with a square lattice overlaying the electron micrographs by counting the number of points within the compartment (point hit method, Griffiths, 1993). The mesh size of the square lattice was adjusted to the magnification of the electron micrographs: 7.5, 10.28, and 12.45 mm for magnifications of 30,000×, 40,000×, and 49,000×, respectively. The labeling density of cathepsin D was calculated by dividing the number of gold particles for cathepsin D by the product of the number of points and the area associated with one point (0.0088 μm^2). In this way the numerical density of gold over an area was obtained in gold particles per μm^2 (Griffiths, 1993). The size of the secretory granules in wild-type and *Gnptab* −/− pancreatic acinar cells was determined by using the same point hit method. In total, 165 and 211 secretory granules were evaluated in the wild-type and *Gnptab* −/−, respectively. P values were determined by performing a *t* test.

ACKNOWLEDGMENTS

We thank all our colleagues for their advice, as well as Marc van Peski and René Scriwanek for their photographical expertise and Wang-Sik Lee for his help with the cathepsin D Western blotting. E.v.M. is supported by VICI grant 918.56.611 of the Netherlands Organization for Scientific Research (NWO), awarded to J.K. M.B. and S.K. are supported by NIH grant CA-008759–44.

REFERENCES

Aniento F, Roche E, Cuervo AM, Knecht E (1993). Uptake and degradation of glyceraldehyde-3-phosphate dehydrogenase by rat liver lysosomes. J Biol Chem 268, 10463–10470.

Aula P, Rapola J, Autio S, Raivio K, Karjalainen O (1975). Prenatal diagnosis and fetal pathology of I-cell disease (mucolipidosis type II). J Pediatr 87, 221–226.

Boonen M, Vogel P, Platt KA, Dahms N, Kornfeld S (2009). Mice lacking mannose 6-phosphate uncovering enzyme activity have a milder phenotype than mice deficient for N-acetylglucosamine-1-phosphotransferase activity. Mol Biol Cell 20, 4381–4389.
Cao Y, Klionsky DJ (2007). Physiological functions of Atg6/Beclin 1: a unique autophagy-related protein. Cell Res 17, 839–849.
Cathey SS, Leroy JG, Wood T, Eaves K, Simensen RJ, Kudo M, Stevenson RE, Friez MJ (2010). Phenotype and genotype in mucolipidosis II and III alpha/beta: a study of 61 probands. J Med Genet 47, 38–48.
Cuervo AM (2004). Autophagy: many paths to the same end. Mol Cell Biochem 263, 55–72.
Dittié AS, Klumperman J, Tooze SA (1999). Differential distribution of mannose 6-phosphate receptors and furin in immature secretory granules. J Cell Sci 112, 3955–3966.
Dittmer F, Ulbrich EJ, Hafner A, Schmahl W, Meister T, Pohlmann R, von Figura K (1999). Alternative mechanisms for trafficking of lysosomal enzymes in mannose 6-phosphate receptor-deficient mice are cell type-specific. J Cell Sci 112, 1591–1597.
Elleder M, Martin JJ (1998). Mucolipidosis type II with evidence of a novel storage site. Virchows Arch 433, 575–578.
Fraldi A *et al.* (2010). Lysosomal fusion and SNARE function are impaired by cholesterol accumulation in lysosomal storage disorders. EMBO J 29, 3607–3620.
Gelfman C, Vogel P, Issa TM, Turner A, Lee WS, Kornfeld S, Rice DS (2007). Mice lacking α/β subunits of GlcNAc-1-phosphotransferase exhibit growth retardation, retinal degeneration, and secretory cell lesions. Invest Ophthalmol Vis Sci 48, 5221–5228.
Glickman JN, Kornfeld S (1993). Mannose 6-phosphate-independent targeting of lysosomal enzymes in I-cell disease B lymphoblasts. J Cell Biol 123, 99–108.
Glickman JN, Morton PA, Slot JW, Kornfeld S, Geuze HJ (1996). The biogenesis of the MHC class II compartment in human I-cell disease B lymphoblasts. J Cell Biol 132, 769–785.
Griffiths G (1993). Quantitative aspects of immunocytochemistry. Fine Structure Immunocytochemistry Berlin, Heidelberg: Springer-Verlag, 371–445.
Hickman S, Neufeld EF (1972). A hypothesis for I-cell disease: defective hydrolases that do not enter lysosomes. Biochem Biophys Res Commun 49, 992–999.
Jung CH, Ro SH, Cao J, Otto NM, Kim DH (2010). mTOR regulation of autophagy. FEBS Lett 584, 1287–1295.
Kenyon KR, Sensenbrenner JA (1971). Mucolipidosis II (I-cell disease): ultrastructural observations of conjunctiva and skin. Invest Ophthalmol 10, 555–567.
Kenyon KR, Sensenbrenner JA, Wyllie RG (1973). Hepatic ultrastructure and and histochemistry in mucolipidosis II (I-cell disease). Pediatr Res 7, 560–568.
Klumperman J, Kuliawat R, Griffith JM, Geuze HJ, Arvan P (1998). Mannose 6-phosphate receptors are sorted from immature secretory granules via adaptor protein AP-1, clathrin, and syntaxin 6-positive vesicles. J Cell Biol 141, 359–371.
Kollmann K *et al.* (2010). Mannose phosphorylation in health and disease. Eur J Cell Biol 89, 117–123.
Kornfeld S, Sly WS (2000). I-cell disease and pseudo-Hurler polydystrophy: disorders of lysosomal enzyme phosphorylation and localization. In: The Metabolic and Molecular Bases of Inherited Disease, eds. CR Scriver *et al.,* New York: McGraw-Hill, 3469–3483.
Korolchuk VI, Mansilla A, Menzies FM, Rubinsztein DC (2009). Autophagy inhibition compromises degradation of ubiquitin-proteasome pathway substrates. Mol Cell 33, 517–527.
Kuliawat R, Arvan P (1994). Distinct molecular mechanisms for protein sorting within immature secretory granules of pancreatic beta-cells. J Cell Biol 126, 77–86.
Kuliawat R, Klumperman J, Ludwig T, Arvan P (1997). Differential sorting of lysosomal enzymes out of the regulated secretory pathway in pancreatic beta-cells. J Cell Biol 137, 595–608.
Lee WS, Payne BJ, Gelfman CM, Vogel P, Kornfeld S (2007). Murine UDP-GlcNAc:lysosomal enzyme N-acetylglucosamine-1-phosphotransferase lacking the gamma-subunit retains substantial activity toward acid hydrolases. J Biol Chem 282, 27198–27203.
Leroy JG, Demars RI (1967). Mutant enzymatic and cytological phenotypes in cultured human fibroblasts. Science 157, 804–806.
Leroy JG, Ho MW, MacBrinn MC, Zielke K, Jacob J, O'Brien JS (1972). I-cell disease: biochemical studies. Pediatr Res 6, 752–757.
Lightbody J, Wiesmann U, Hadorn B, Herschkowitz N (1971). I-cell disease: multiple lysosomal-enzyme defect. Lancet 1, 451.
Magini A, Mencarelli S, Tancini B, Ciccarone V, Urbanelli L, Hasilik A, Emiliani C (2008). Identification and characterization of mature beta-hexosaminidases associated with human placenta lysosomal membrane. Biosci Rep 28, 229–237.
Martin JJ, Leroy JG, Farriaux JP, Fontaine G, Desnick RJ, Cabello A (1975). I-cell disease (mucolipidosis II). A report on its pathology. Acta Neuropathol (Berl) 33, 285–305.
Martin JJ, Leroy JG, Van Eygen M, Ceuterick C (1984). I-cell disease. A further report on its pathology. Acta Neuropathol (Berl) 64, 234–242.
Meister T, Niehues R, Hahn D, Domschke W, Sendler M, Lerch MM, Schnekenburger J (2010). Missorting of cathepsin B into the secretory compartment of CI-MPR/IGFII-deficient mice does not induce spontaneous trypsinogen activation but leads to enhanced trypsin activity during experimental pancreatitis—without affecting disease severity. J Physiol Pharmacol 61, 565–575.
Mizushima N, Yamamoto A, Matsui M, Yoshimori T, Ohsumi Y (2004). In vivo analysis of autophagy in response to nutrient starvation using transgenic mice expressing a fluorescent autophagosome marker. Mol Biol Cell 15, 1101–1111.
Nagashima K, Sakakibara K, Endo H, Konishi Y, Nakamura N, Suzuki Y, Abe T (1977). I-cell disease (mucolipidosis II). Pathological and biochemical studies of an autopsy case. Acta Pathol Jpn 27, 251–264.
Otomo T, Higaki K, Nanba E, Ozono K, Sakai N (2009). Inhibition of autophagosome formation restores mitochondrial function in mucolipidosis II and III skin fibroblasts. Mol Genet Metab 98, 393–399.
Owada M, Neufeld EF (1982). Is there a mechanism for introducing acid hydrolases into liver lysosomes that is independent of mannose 6-phosphate recognition? Evidence from I-cell disease. Biochem Biophys Res Commun 105, 814–820.
Pattingre S, Espert L, Biard-Piechaczyk M, Codogno P (2008). Regulation of macroautophagy by mTOR and Beclin 1 complexes. Biochimie 90, 313–323.
Pohl S, Marschner K, Storch S, Braulke T (2009). Glycosylation- and phosphorylation-dependent intracellular transport of lysosomal hydrolases. Biol Chem 390, 521–527.
Reczek D, Schwake M, Schröder J, Hughes H, Blanz J, Jin X, Brondyk W, Van Patten S, Edmunds T, Saftig P (2007). LIMP-2 is a receptor for lysosomal mannose-6-phosphate-independent targeting of beta-glucocerebrosidase. Cell 131, 770–783.
Sardiello M *et al.* (2009). A gene network regulating lysosomal biogenesis and function. Science 325, 473–477.
Settembre C, Fraldi A, Jahreiss L, Spampanato C, Venturi C, Medina D, de Pablo R, Tacchetti C, Rubinsztein DC, Ballabio A (2008). A block of autophagy in lysosomal storage disorders. Hum Mol Genet 17, 119–129.
Sleat DE, Della Valle MC, Zheng H, Moore DF, Lobel P (2008). The mannose 6-phosphate glycoprotein proteome. J Proteome Res 7, 3010–3021.
Slot JW, Geuze HJ (2007). Cryosectioning and immunolabeling. Nat Protoc 2, 2480–2491.
Smith RE, Farquhar MG (1966). Lysosome function in the regulation of the secretory process in cells of the anterior pituitary gland. J Cell Biol 31, 319–347.
Tondeur M, Vamos-Hurwitz E, Mockel-Pohls S, Dereume JP, Cremer N, Loeb H (1971). Clinical, biochemical, and ultrastructural studies in a case of chondrodystrophy presenting the I-cell phenotype in culture. J Pediatr 79, 366–378.
Tooze J, Tooze SA (1986). Clathrin-coated vesicular transport of secretory proteins during the formation of ACTH-containing secretory granules in AtT20 cells. J Cell Biol 103, 839–850.
Vogel P, Payne BJ, Read R, Lee WS, Gelfman CM, Kornfeld S (2009). Comparative pathology of murine mucolipidosis types II and IIIC. Vet Pathol 46, 313–324.
Waheed A, Pohlman R, Hasilik A, von Figura K, Elsen AV, Leroy JG (1982). Deficiency of UDP-N-acetylglucosamine:lysosomal enzyme N-acetylglucosamine-1-phosphotransferase in organs of I-cell patients. Biochem Biophys Res Commun 105, 1052–1058.
Wiesmann UN, Lightbody J, Vasella F, Herschkowitz N (1971a). Multiple enzyme deficiency due to enzyme leakage? New Engl J Med 284, 109–110.
Wiesmann U, Vasella F, Herschkowitz N (1971b). I-cell disease: leakage of lysosomal enzymes into extracellular fluids. New Engl J Med 285, 1090–1091.
Yadao F,, Hechtman P, Kaplan F (1997). Formation of a ternary complex between GM2 activator protein, GM2 ganglioside and hexosaminidase A. Biochim Biophys Acta 1340, 45–52.
Yu L *et al.* (2010). Autophagy termination and lysosome reformation regulated by mTOR. Nature 465, 942–946.